

The dependence of phase functions of large transparent particles on their refractive index and shape

A A Kokhanovsky[†] and T Y Nakajima[‡]

[†] Institute of Particle Technology and Environmental Engineering,
Clausthal Technical University, Leibnizstrasse 19, D-38678 Clausthal-Zellerfeld,
Germany

[‡] Earth Observation Research Centre, National Space Development Agency of
Japan, 1-9-9 Roppongi, Minato-ku, Tokyo 106, Japan

Received 5 January 1998, in final form 23 February 1998

Abstract. A new, fast ray tracing code for calculating local optical characteristics of light-scattering media with large particles was created. The dependences of phase functions of nonabsorbing particles on their shape and refractive index were investigated. It was found that the position of the primary rainbow can be used to retrieve the aspect ratio of spheroidal particles.

1. Introduction

The phase function $p(\Omega)$ is one of the most important characteristics of light-scattering media. It determines the angular distribution of the singly scattered radiation and is normalized by the following condition [1]:

$$\frac{1}{4\pi} \int_{4\pi} p(\Omega) d\Omega = 1. \quad (1)$$

Thus, one can see that the phase function is equal to the probability of photon scattering in the direction characterized by the solid angle Ω . This probability depends on the shape, size and refractive index $m = m_r - im_i$ of particles. For randomly oriented particles, $p(\Omega)$ does not depend on the azimuth ϕ and equation (1) can be simplified to

$$\frac{1}{2} \int_0^\pi p(\theta) \sin \theta d\theta = 1 \quad (2)$$

where we used the equality $d\Omega = 2\pi \sin \theta d\theta$. Here θ is the scattering angle.

To obtain the phase function of a single particle one should solve Maxwell equations with corresponding boundary conditions and the conditions to be satisfied at infinity. This could be done by various means, including by the method of separation of variables [2–4], the T-matrix method [5,6], the finite difference method [7] and others [8]. The common feature of all these methods is that computations become more and more complex for smaller values of the ratio λ/a , where a is the characteristic dimension of a particle and λ is the wavelength of the

incident radiation. In addition, calculated phase functions approach asymptotical patterns, which do not depend on the size of particles, except for very-narrow-angle regions with high intensities of scattered light (forwards, glory and rainbow scattering [9]).

The task of this paper is to calculate these size-independent patterns for spheres and for oblate and prolate spheroids with various refractive indices. We use the geometrical optics approach (GOA) in our calculations [9,10]. It is based on the well-known correspondence between Maxwell and geometrical optics equations at $\lambda \rightarrow 0$ [10]. Actually, at short wavelengths ($\lambda \ll a$) the incident wave can be represented as a collection of independent rays. The history of each ray incident on the particle surface is traced using Snell's law and Fresnel's equations [10].

This approximation has already been applied successfully for calculating phase functions of large spheres [9], spheroids [11], polyhedral ice crystals [12], hexagonal cylinders [13] and particles with stochastic surfaces [14]. In most cases, only particles with fixed values of the refractive index were considered, corresponding to the optical constants of water, dust and ice. Our calculations cover a wider range of optical constants. Moreover, we present our results in tables, which allow them to be used by a wider audience.

2. The method of computation

The most important part of any ray-tracing code is a definition of a surface of a light-scattering particle. The

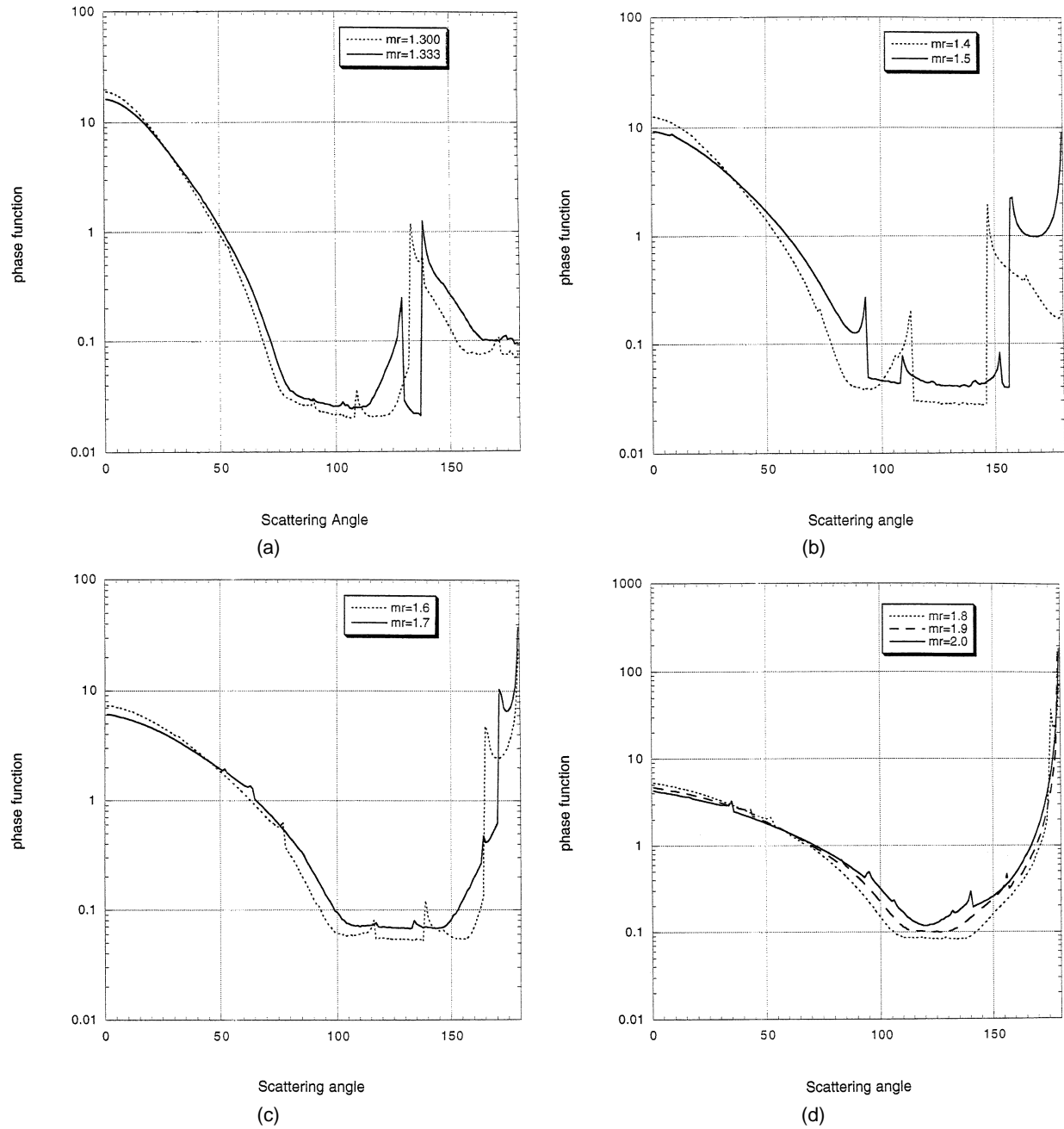


Figure 1. Phase functions of large transparent spheres with refractive indices $m = 1.3$ and 1.333 (a), 1.4 and 1.5 (b), 1.6 and 1.7 (c) and 1.8 , 1.9 and 2.0 (d).

surface could be defined in various ways. In our new computation code [15], we represent every surface element as a spherical surface with a large radius. For example, cubic and hexagonal columns are composed of six and eight surfaces, respectively, and each surface in our computation code is represented by a spherical surface with a large radius. Such an approach allows us to calculate phase functions of particles with different shapes in the framework of the same algorithm.

We associate with each incident photon a random number $0 \leq l \leq 1$. Only photons with $l > R$ have a chance to penetrate into particles. ‘Low-energy’ photons ($l \leq R$) are reflected by the surface of a particle. Note that

the value of R is calculated with the Fresnel formulae and represents the fraction of photons that is reflected rather than refracted. The value of R depends on the polarization state of the incident light. For instance, in the case of the incident natural light and transparent particles, considered in this paper, it follows that $R = 0.5(R_1^2 + R_2^2)$, where $R_j = (m^{(-1)^j} \cos \phi - \cos \psi) / (m^{(-1)^j} \cos \phi + \cos \psi)$, $j = 1$ or 2 , ϕ is the angle of incidence and ψ is the angle of refraction, determined by Snell’s law $\sin \psi = \sin \phi / m$. Thus, R depends on the point of interaction (the angle ϕ) and the refractive index m . In the case of total reflection (the angle of refraction is complex) only the reflected ray is traced.

Table 1. Phase functions of large transparent spheres.

θ	m					
	1.1	1.2	1.3	1.333	1.4	1.5
0.0	1.201×10^2	3.631×10^1	1.911×10^1	1.635×10^1	1.264×10^1	9.232
1.0	1.184×10^2	3.610×10^1	1.905×10^1	1.634×10^1	1.260×10^1	9.239
2.0	1.128×10^2	3.547×10^1	1.883×10^1	1.612×10^1	1.244×10^1	9.189
3.0	1.042×10^2	3.477×10^1	1.857×10^1	1.593×10^1	1.231×10^1	9.074
4.0	9.378×10^1	3.365×10^1	1.830×10^1	1.572×10^1	1.211×10^1	8.976
5.0	8.252×10^1	3.235×10^1	1.791×10^1	1.545×10^1	1.200×10^1	8.877
10.0	3.583×10^1	2.394×10^1	1.532×10^1	1.346×10^1	1.079×10^1	8.843
20.0	6.085	9.765	9.012	8.531	7.548	6.318
30.0	1.183	3.595	4.597	4.671	4.644	4.349
40.0	1.572×10^{-1}	1.245	2.170	2.416	2.640	2.794
50.0	2.303×10^{-2}	3.474×10^{-1}	9.528×10^{-1}	1.112	1.400	1.692
60.0	1.321×10^{-2}	5.804×10^{-2}	3.273×10^{-1}	4.423×10^{-1}	6.664×10^{-1}	9.435×10^{-1}
70.0	8.006×10^{-3}	2.234×10^{-2}	7.959×10^{-2}	1.259×10^{-1}	2.541×10^{-1}	4.654×10^{-1}
80.0	6.203×10^{-3}	1.638×10^{-2}	2.939×10^{-2}	3.543×10^{-2}	7.428×10^{-2}	1.992×10^{-1}
90.0	7.941×10^{-2}	1.308×10^{-2}	2.893×10^{-2}	2.953×10^{-2}	3.937×10^{-2}	1.325×10^{-1}
100.0	1.375×10^{-2}	3.591×10^{-2}	2.132×10^{-2}	2.588×10^{-2}	4.541×10^{-2}	4.620×10^{-2}
110.0	8.756×10^{-3}	9.526×10^{-3}	2.693×10^{-2}	2.505×10^{-2}	9.975×10^{-2}	6.317×10^{-2}
120.0	6.834×10^{-3}	1.643×10^{-1}	2.069×10^{-2}	4.355×10^{-2}	2.908×10^{-2}	4.356×10^{-2}
130.0	7.918×10^{-3}	4.032×10^{-2}	4.435×10^{-2}	2.870×10^{-2}	2.850×10^{-2}	4.135×10^{-2}
140.0	7.674×10^{-2}	2.981×10^{-2}	2.913×10^{-1}	6.154×10^{-1}	2.787×10^{-2}	4.462×10^{-2}
150.0	8.070×10^{-3}	3.106×10^{-2}	1.280×10^{-1}	2.600×10^{-1}	7.118×10^{-1}	5.252×10^{-2}
160.0	7.821×10^{-3}	3.502×10^{-2}	7.645×10^{-2}	1.230×10^{-1}	4.260×10^{-1}	1.315
170.0	1.120×10^{-1}	3.700×10^{-1}	1.031×10^{-1}	9.925×10^{-2}	2.573×10^{-1}	9.937×10^{-1}
180.0	1.368×10^{-1}	3.148×10^{-2}	7.756×10^{-2}	1.012×10^{-1}	1.840×10^{-1}	8.672

θ	m				
	1.6	1.7	1.8	1.9	2.0
0.0	7.319	6.073	5.263	4.624	4.324
1.0	7.316	6.068	5.224	4.603	4.249
2.0	7.263	6.039	5.182	4.562	4.175
3.0	7.201	5.991	5.146	4.511	4.152
4.0	7.130	5.910	5.069	4.451	4.106
5.0	7.050	5.859	5.020	4.395	4.048
10.0	6.610	5.510	4.735	4.150	3.847
20.0	5.343	4.608	4.054	3.630	3.350
30.0	3.974	3.619	3.303	3.069	2.942
40.0	2.796	2.679	2.597	2.566	2.261
50.0	1.838	1.924	2.035	1.845	1.803
60.0	1.160	1.379	1.348	1.375	1.393
70.0	6.994×10^{-1}	7.994×10^{-1}	9.556×10^{-1}	9.835×10^{-1}	1.042
80.0	3.160×10^{-1}	4.551×10^{-1}	5.763×10^{-1}	6.603×10^{-1}	7.408×10^{-1}
90.0	1.246×10^{-1}	2.151×10^{-1}	3.126×10^{-1}	4.211×10^{-1}	4.882×10^{-1}
100.0	6.103×10^{-2}	9.463×10^{-2}	1.470×10^{-1}	2.177×10^{-1}	3.125×10^{-1}
110.0	5.988×10^{-2}	7.060×10^{-2}	8.609×10^{-2}	1.118×10^{-1}	1.677×10^{-1}
120.0	5.480×10^{-2}	6.887×10^{-2}	8.839×10^{-2}	9.901×10^{-2}	1.169×10^{-1}
130.0	5.450×10^{-2}	6.831×10^{-2}	8.384×10^{-2}	1.001×10^{-1}	1.488×10^{-1}
140.0	8.389×10^{-2}	6.971×10^{-2}	8.922×10^{-2}	1.422×10^{-1}	2.886×10^{-1}
150.0	5.698×10^{-2}	8.143×10^{-2}	1.644×10^{-1}	2.337×10^{-1}	2.573×10^{-1}
160.0	7.070×10^{-2}	2.000×10^{-1}	3.038×10^{-1}	3.886×10^{-1}	4.726×10^{-1}
170.0	2.416	6.213×10^{-1}	8.678×10^{-1}	1.112	1.620
180.0	2.385×10^1	3.751×10^1	7.219×10^1	2.010×10^2	1.837×10^2

At the next interaction point we compare R and l again and repeat the whole procedure. When there is no interaction point the next interaction point and particle rotations are determined by a random number.

Note that our code can be used to calculate phase matrices both of single particles and of their assemblies

[15]. Distributions of shapes, orientations and sizes of particles can be taken into account.

In this paper we will consider our results for the first element of the phase matrix, namely the phase function. Results for the phase matrices of spheroids, spheres and hexagonal columns, obtained with our code, one can find in [15].

Table 2. Phase functions of large transparent oblate (4 : 4 : 3) spheroids.

θ	m					
	1.1	1.2	1.3	1.333	1.4	1.5
0.0	1.231×10^2	3.749×10^1	1.990×10^1	1.761×10^1	1.318×10^1	9.917
1.0	1.215×10^2	3.736×10^1	1.989×10^1	1.746×10^1	1.315×10^1	9.886
2.0	1.151×10^2	3.672×10^1	1.969×10^1	1.720×10^1	1.307×10^1	9.797
3.0	1.057×10^2	3.576×10^1	1.940×10^1	1.692×10^1	1.292×10^1	9.682
4.0	9.452×10^1	3.456×10^1	1.905×10^1	1.663×10^1	1.273×10^1	9.554
5.0	8.272×10^1	3.313×10^1	1.864×10^1	1.627×10^1	1.254×10^1	9.447
10.0	3.561×10^1	2.418×10^1	1.575×10^1	1.404×10^1	1.122×10^1	8.651
20.0	6.191	9.767	9.149	8.651	7.746	6.542
30.0	1.078	3.496	4.542	4.603	4.623	4.376
40.0	7.429×10^{-2}	9.947×10^{-1}	1.924	2.140	2.422	2.611
50.0	2.704×10^{-2}	1.471×10^{-1}	5.552×10^{-1}	7.178×10^{-1}	1.004	1.279
60.0	1.336×10^{-2}	4.928×10^{-2}	1.177×10^{-1}	1.811×10^{-1}	3.140×10^{-1}	4.528×10^{-1}
70.0	9.146×10^{-3}	3.048×10^{-2}	5.596×10^{-2}	6.831×10^{-2}	8.490×10^{-2}	1.870×10^{-1}
80.0	1.203×10^{-1}	2.008×10^{-2}	5.015×10^{-2}	4.688×10^{-2}	4.692×10^{-2}	8.560×10^{-2}
90.0	4.146×10^{-2}	1.432×10^{-2}	2.699×10^{-2}	3.257×10^{-2}	3.872×10^{-2}	7.152×10^{-2}
100.0	1.595×10^{-2}	2.510×10^{-1}	2.337×10^{-2}	2.888×10^{-2}	3.728×10^{-2}	8.500×10^{-2}
110.0	8.775×10^{-3}	1.402×10^{-1}	4.064×10^{-1}	4.588×10^{-1}	5.361×10^{-2}	1.262×10^{-1}
120.0	9.956×10^{-2}	7.373×10^{-2}	2.889×10^{-1}	3.839×10^{-1}	5.679×10^{-1}	7.343×10^{-1}
130.0	3.537×10^{-2}	3.942×10^{-2}	1.989×10^{-1}	2.961×10^{-1}	5.089×10^{-1}	6.208×10^{-1}
140.0	1.853×10^{-2}	3.313×10^{-2}	1.742×10^{-1}	2.406×10^{-1}	3.089×10^{-1}	5.340×10^{-1}
150.0	8.887×10^{-3}	3.755×10^{-2}	1.065×10^{-1}	1.300×10^{-1}	2.871×10^{-1}	4.108×10^{-1}
160.0	9.610×10^{-3}	1.641×10^{-1}	1.551×10^{-1}	1.167×10^{-1}	1.945×10^{-1}	4.844×10^{-1}
170.0	1.214×10^{-1}	3.867×10^{-1}	1.247×10^{-1}	1.567×10^{-1}	2.869×10^{-1}	4.445×10^{-1}
180.0	1.077×10^{-1}	2.379×10^{-1}	1.496×10^{-1}	2.407×10^{-1}	1.369	1.120

θ	m				
	1.6	1.7	1.8	1.9	2.0
0.0	7.935	6.691	5.769	5.182	4.709
1.0	7.896	6.678	5.731	5.142	4.690
2.0	7.850	6.590	5.704	5.095	4.655
3.0	7.756	6.531	5.641	5.052	4.580
4.0	7.666	6.455	5.573	5.000	4.537
5.0	7.573	6.380	5.515	4.944	4.456
10.0	7.037	5.946	5.136	4.587	4.152
20.0	5.616	4.903	4.396	4.032	3.846
30.0	4.032	3.705	3.466	3.192	2.974
40.0	2.612	2.539	2.420	2.293	2.154
50.0	1.426	1.499	1.512	1.486	1.448
60.0	6.057×10^{-1}	7.283×10^{-1}	8.126×10^{-1}	8.308×10^{-1}	8.538×10^{-1}
70.0	2.386×10^{-1}	3.254×10^{-1}	3.803×10^{-1}	4.496×10^{-1}	5.098×10^{-1}
80.0	1.293×10^{-1}	1.621×10^{-1}	2.344×10^{-1}	3.067×10^{-1}	3.737×10^{-1}
90.0	1.288×10^{-1}	1.535×10^{-1}	2.379×10^{-1}	3.370×10^{-1}	4.282×10^{-1}
100.0	1.571×10^{-1}	2.717×10^{-1}	3.668×10^{-1}	4.160×10^{-1}	5.198×10^{-1}
110.0	2.377×10^{-1}	3.517×10^{-1}	4.906×10^{-1}	6.054×10^{-1}	5.072×10^{-1}
120.0	2.721×10^{-1}	2.178×10^{-1}	1.085×10^{-1}	1.622×10^{-1}	1.869×10^{-1}
130.0	7.355×10^{-1}	7.501×10^{-1}	2.261×10^{-1}	1.212×10^{-1}	1.799×10^{-1}
140.0	7.155×10^{-1}	8.615×10^{-1}	9.413×10^{-1}	9.728×10^{-1}	9.639×10^{-1}
150.0	6.373×10^{-1}	8.323×10^{-1}	1.000	1.122	1.207
160.0	5.307×10^{-1}	7.265×10^{-1}	9.969×10^{-1}	1.225	1.401
170.0	7.646×10^{-1}	1.368	1.194	1.261	1.508
180.0	1.336	1.842	2.523	5.193	4.067

3. Results of numerical calculations

According to [9], the phase function of large particles can be represented by the following equation:

$$p(\theta) = \frac{p^d(\theta)\sigma_{sca}^d + p^g(\theta)\sigma_{sca}^g}{\sigma_{sca}^d + \sigma_{sca}^g} \quad (3)$$

where $p^d(\theta)$ and σ_{sca}^d are components of the phase function and scattering cross section resulting from the diffraction process on the boundary of a particle and values of $p^g(\theta)$ and σ_{sca}^g are geometrical optics parts of the scattered light field. The value of σ_{sca}^d is equal to the total geometrical cross section of a particle in a plane which is perpendicular to the incident radiation [9] and the phase function $p^d(\theta)$

Table 3. Phase functions of large transparent prolate (5 : 4 : 4) spheroids.

θ	m					
	1.1	1.2	1.3	1.333	1.4	1.5
0.0	1.304×10^2	3.870×10^1	2.007×10^1	1.720×10^1	1.296×10^1	9.505
1.0	1.285×10^2	3.846×10^1	2.000×10^1	1.718×10^1	1.298×10^1	9.445
2.0	1.218×10^2	3.793×10^1	1.983×10^1	1.706×10^1	1.284×10^1	9.398
3.0	1.116×10^2	3.700×10^1	1.956×10^1	1.682×10^1	1.276×10^1	9.290
4.0	9.928×10^1	3.576×10^1	1.923×10^1	1.655×10^1	1.260×10^1	9.200
5.0	8.626×10^1	3.419×10^1	1.881×10^1	1.625×10^1	1.239×10^1	9.091
10.0	3.556×10^1	2.460×10^1	1.581×10^1	1.395×10^1	1.106×10^1	8.349
20.0	5.809	9.546	8.988	8.514	7.542	6.280
30.0	1.066	3.376	4.396	4.496	4.469	4.214
40.0	9.551×10^{-2}	1.077	1.982	2.180	2.430	2.611
50.0	2.619×10^{-2}	2.321×10^{-1}	7.455×10^{-1}	9.088×10^{-1}	1.178	1.482
60.0	1.332×10^{-2}	4.604×10^{-2}	1.702×10^{-1}	2.548×10^{-1}	4.587×10^{-1}	6.669×10^{-1}
70.0	8.776×10^{-3}	2.324×10^{-2}	5.136×10^{-2}	7.908×10^{-2}	1.420×10^{-1}	2.302×10^{-1}
80.0	9.820×10^{-2}	1.714×10^{-2}	4.417×10^{-2}	3.666×10^{-2}	5.419×10^{-2}	9.393×10^{-2}
90.0	5.562×10^{-2}	1.416×10^{-2}	3.081×10^{-2}	3.162×10^{-2}	5.056×10^{-2}	1.102×10^{-1}
100.0	1.433×10^{-2}	1.952×10^{-1}	2.548×10^{-2}	2.877×10^{-2}	4.710×10^{-2}	6.709×10^{-2}
110.0	9.596×10^{-3}	1.549×10^{-1}	2.271×10^{-1}	3.061×10^{-2}	1.003×10^{-1}	8.428×10^{-2}
120.0	1.649×10^{-2}	9.025×10^{-2}	3.189×10^{-1}	3.778×10^{-1}	3.576×10^{-1}	5.047×10^{-2}
130.0	4.696×10^{-2}	4.037×10^{-2}	2.806×10^{-1}	4.748×10^{-1}	5.342×10^{-1}	5.940×10^{-1}
140.0	2.227×10^{-2}	3.305×10^{-2}	2.910×10^{-1}	3.419×10^{-1}	4.690×10^{-1}	7.954×10^{-1}
150.0	9.101×10^{-3}	3.353×10^{-2}	2.061×10^{-1}	1.485×10^{-1}	3.789×10^{-1}	7.283×10^{-1}
160.0	1.397×10^{-1}	4.646×10^{-1}	8.488×10^{-2}	1.160×10^{-1}	2.442×10^{-1}	6.277×10^{-1}
170.0	1.319×10^{-1}	2.486×10^{-1}	8.021×10^{-2}	1.214×10^{-1}	2.199×10^{-1}	4.838×10^{-1}
180.0	4.260×10^{-2}	8.906×10^{-2}	7.591×10^{-2}	1.120×10^{-1}	3.684×10^{-1}	2.360

θ	m				
	1.6	1.7	1.8	1.9	2.0
0.0	7.437	6.076	5.165	4.579	4.080
1.0	7.410	6.058	5.158	4.558	4.066
2.0	7.359	6.048	5.121	4.484	4.040
3.0	7.280	5.977	5.067	4.465	3.970
4.0	7.218	5.914	5.014	4.387	3.909
5.0	7.121	5.846	4.959	4.340	3.857
10.0	6.658	5.483	4.663	4.065	3.626
20.0	5.301	4.521	3.939	3.485	3.142
30.0	3.831	3.467	3.135	2.862	2.625
40.0	2.590	2.481	2.351	2.243	2.089
50.0	1.622	1.653	1.673	1.627	1.573
60.0	8.458×10^{-1}	1.035	1.059	1.088	1.105
70.0	3.730×10^{-1}	4.951×10^{-1}	6.138×10^{-1}	6.565×10^{-1}	7.206×10^{-1}
80.0	1.577×10^{-1}	2.270×10^{-1}	3.315×10^{-1}	4.286×10^{-1}	5.279×10^{-1}
90.0	1.135×10^{-1}	1.617×10^{-1}	2.351×10^{-1}	3.386×10^{-1}	4.043×10^{-1}
100.0	1.054×10^{-1}	1.588×10^{-1}	1.915×10^{-1}	2.360×10^{-1}	3.009×10^{-1}
110.0	8.785×10^{-2}	9.031×10^{-2}	1.152×10^{-1}	1.292×10^{-1}	1.581×10^{-1}
120.0	6.293×10^{-2}	7.869×10^{-2}	1.054×10^{-1}	1.315×10^{-1}	1.521×10^{-1}
130.0	6.036×10^{-2}	7.757×10^{-2}	9.491×10^{-2}	1.568×10^{-1}	2.496×10^{-1}
140.0	1.025	9.477×10^{-1}	9.917×10^{-2}	1.568×10^{-1}	2.496×10^{-1}
150.0	1.199	1.747	2.307	2.640	2.417
160.0	9.072×10^{-1}	1.198	1.469	1.804	2.175
170.0	9.850×10^{-1}	1.457	1.588	1.851	2.148
180.0	2.472	3.215	4.722	7.774	6.969

depends on the shape of this cross section [10, 16]. For spherical particles with radius a , one obtains [9]

$$p^d(\theta) = \frac{4J_1^2(\theta\rho)}{\theta^2} \quad \sigma_{sca}^d = \pi a^2 \quad (4)$$

where $J_1(\theta\rho)$ is the Bessel function, $\rho = 2\pi a/\lambda \gg 1$ and $2\rho(m-1) \gg 1$. Diffraction patterns for other shapes can be found elsewhere [10, 16].

Thus, the main task of this paper is to find the function $p^g(\theta)$ for large transparent (the refractive index is real) particles. In this case, $\sigma_{sca}^g = \sigma_{sca}^d$ [9] and

$$p(\theta) = \frac{1}{2}(p^d(\theta) + p^g(\theta)). \quad (5)$$

Note that $p^d(\theta) \ll p^g(\theta)$ at $\theta \gg 7/\rho$ [9]. The phase functions of large absorbing ($4m_i\rho \gg 1$) randomly oriented

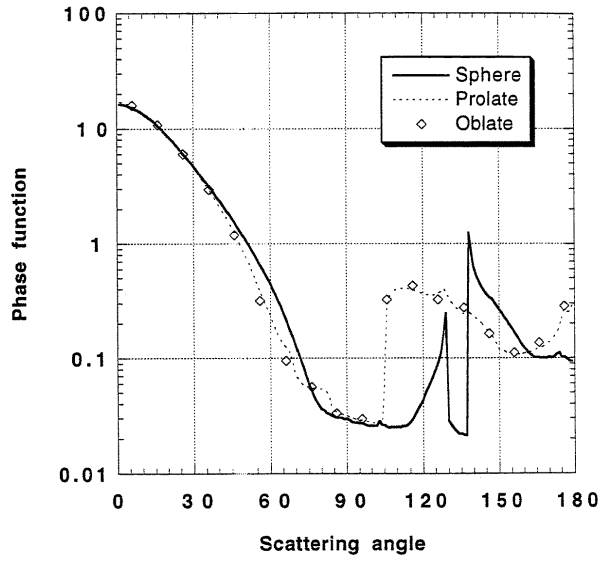


Figure 2. Phase functions of large transparent spheres and of randomly oriented prolate (ratio of axes 3 : 3 : 4) and oblate (ratio of axes 3 : 4 : 4) spheroids with the refractive index $m = 1.333$.

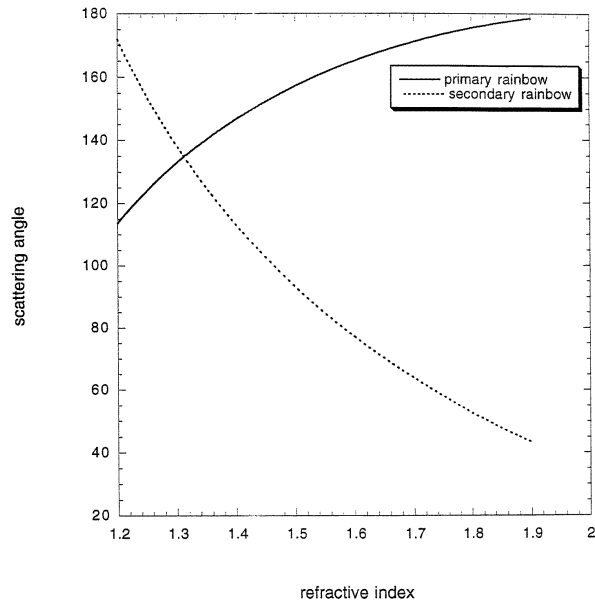
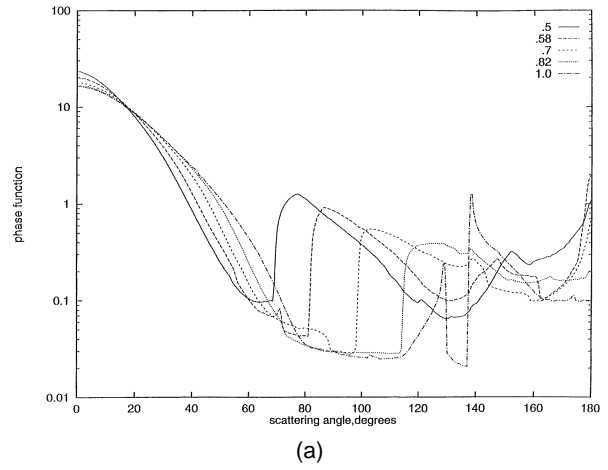


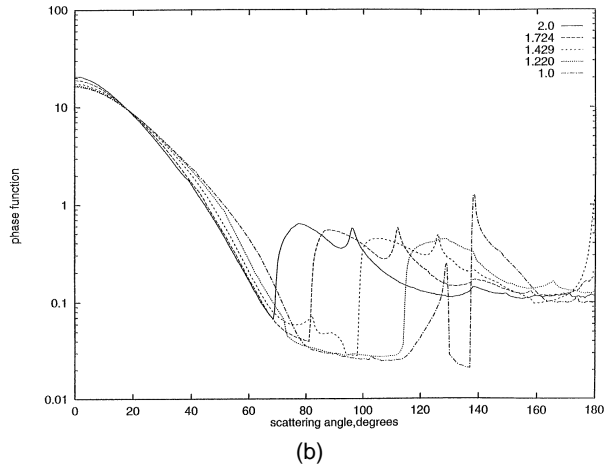
Figure 3. Angles of primary and secondary rainbows for spheres as functions of the refractive index m .

convex particles coincide with those of spheres and are not considered in this paper.

The results of calculations of functions $p^s(\theta)$ for spheres and for prolate and oblate spheroids with random orientations for unpolarized incident light are presented in tables 1–3 and figures 1–4. They do not depend on the size of particles and wavelength. Note that our values of $p^s(\theta)$ for spheres at $n = 1.333$ coincide (to within about 1%) with results published by Shifrin [17]. His results were obtained by using a different algorithm. Thus, we conclude that the accuracy of our code is high. Let us now discuss the obtained results.



(a)



(b)

Figure 4. Phase functions of oblate (a) and prolate (b) spheroids with $m = 1.333$ for various values of the shape parameter ξ .

The value $p^s(0)$ (see table 1 and figure 1) decreases with the refractive index m and *vice versa* for the value of $p^s(\pi)$. This fact originates from the larger reflection of light by particles at larger differences $m - 1$. Moreover, at n larger than $\sqrt{2}$ the glory ray [9] exists in the framework of the GOA. This is the reason for a peak in the backwards direction in figure 1(b). The difference between phase functions of oblate and prolate spheroids with the same aspect ratio r (see figure 2), defined as the ratio of the smallest semi-axis of a spheroid to the largest semi-axis, is small (at least, at $r \geq 0.75$).

Another interesting feature is connected with rainbow angles (see figures 1–5). The angles of the primary θ_1 and secondary θ_2 rainbows for spheres can be calculated from the following equations [9]:

$$\begin{aligned}\theta_1 &= 4 \arccos \left(\frac{\cos \tau_2}{m} \right) - 2\tau_2 \\ \theta_2 &= 2\pi - 6 \arccos \left(\frac{\cos \tau_3}{m} \right) + 2\tau_3\end{aligned}\quad (6)$$

where

$$\tau_p = \arcsin \left[\left(\frac{m^2 - 1}{p^2 - 1} \right)^{1/2} \right]. \quad (7)$$

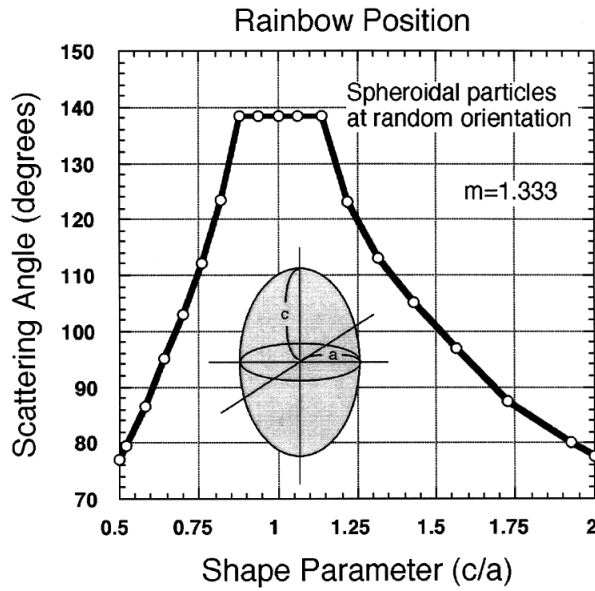


Figure 5. The position of the primary rainbow for spheroids as a function of the shape parameter ξ .

As one can see from figure 3 and equation (6), the positions of the first (θ_1) and the second (θ_2) rainbows coincide at $m = 1.304$. For larger refractive indices, it follows from figure 3 that θ_1 is larger than θ_2 (for example, for water clouds) and θ_1 is smaller than θ_2 for smaller values of n . Note that the angular distance between two rainbows increases with the refractive index of particles at $m > 1.304$ and rainbows almost disappear at $m > 1.7$.

From tables 1–3 it follows that changing the shape of particles from spherical to spheroidal hardly changes the phase function in the forward hemisphere for the shape parameter $\xi \in [0.75, 1.25]$ ($\xi = c/a$, where the semi-axis $a = b < c$ for prolate spheroids and $a = b > c$ for oblate spheroids). Thus, one can conclude that variation of the shape parameter within 25% in practice does not affect the reflected and twice-refracted light.

In contrast, the changes in the backward hemisphere are very prominent. The main rainbow becomes broader and shifts to smaller scattering angles (see figures 4 and 5). The secondary rainbow almost disappears. The overall energy scattered in the backward hemisphere increases in comparison with light scattering by spheres and the value of the asymmetry parameter

$$g = \frac{1}{2} \int_0^\pi p(\theta) \sin \theta \cos \theta d\theta$$

decreases [18]. Phase functions of oblate and prolate spheroids at $r \geq 0.75$ are similar to each other at $\theta \leq \pi/2$.

The positions of the primary rainbow for oblate and prolate spheroids for various values of the shape parameter ξ are presented in figure 5 for $m = 1.333$. One can see that the value of the primary rainbow angle is smaller for spheroids than it is for spheres. It decreases faster for oblate spheroids. The dependence $\theta_1(\xi)$ can be used to estimate the shape parameter of spheroidal particles.

4. Conclusion

Phase functions of large spherical and spheroidal particles were calculated for wide ranges of optical constants and aspect ratios using a newly developed ray-tracing code. It was found that the position of a primary rainbow can be used to estimate the shape of spheroidal particles.

Results obtained can be used as input parameters for multiple scattering calculations and as additional tests of codes based on solutions of Maxwell's equations for $\rho \gg 1$.

Acknowledgments

A Kokhanovsky held Science and Technology of Japan and Alexander von Humboldt fellowships during this research.

References

- [1] Zege E P, Ivanov A P and Katsev I L 1991 *Image Transfer Through a Scattering Medium* (Berlin: Springer)
- [2] Asano S and Yamamoto G 1975 *Appl. Opt.* **14** 29
- [3] Onaka T 1980 *Ann. Tokyo Astron. Obs.* **18** 1
- [4] Farafonov V G 1983 *Differential Equations (Sov.)* **19** 1765
- [5] Waterman P C 1971 *Phys. Rev. D* **3** 825
- [6] Mishchenko M I, Travis L D and Macke A 1996 *Appl. Opt.* **35** 4927
- [7] Kunz K S and Luebbers R J 1993 *The Finite Difference Time Domain Method for Electromagnetics* (Boca Raton, FL: CRC)
- [8] Holt A R 1982 *Radio Sci.* **17** 929
- [9] Van de Hulst H C 1981 *Light Scattering by Small Particles* (New York: Dover)
- [10] Born M and Wolf E 1989 *Principles of Optics* (Oxford: Pergamon)
- [11] Macke A, Mishchenko M I, Muinonen K and Carlson B E 1995 *Opt. Lett.* **20** 1934
- [12] Macke A 1993 *Appl. Opt.* **32** 2780
- [13] Takano Y and Liou K N 1989 *J. Atmos. Sci.* **46** 3
- [14] Peltoniemi J I, Lumme K, Muinonen K and Irvine W M 1989 *Appl. Opt.* **28** 4088
- [15] Nakajima T Y, Nakajima T and Kokhanovsky A A 1998 *Proc. SPIE* **3220** 2
- [16] Bohren C F and Koh G 1985 *Appl. Opt.* **24** 1023
- [17] Shifrin K S 1951 *Rasseyaniye Sveta v Mutnoi Srede* (Moscow: Gostekhteorizdat)
- [18] Kokhanovsky A A and Macke A 1997 *Appl. Opt.* **36** 8785